Extension of the MoM Laplacian Solution to the General Helmholtz Equation

Jalel Rejeb, Tapan Sarkar, *Fellow, IEEE*, and Ercument Arvas, *Senior Member, IEEE*

***Abstract*— A new boundary integral method for solving the general Helmholtz equation has been developed. The new formulation is based on the method of moments Laplacian solution. The main feature of this new formulation is that the boundary conditions are satisfied independent of the region node discretizations. The numerical solution of the present method are compared with finite difference and finite element solutions.**

I. Introduction

THE TWO-DIMENSIONAL Helmholtz's equation appears in a variety of physical phenomena and engineering applications, such as, acoustic radiation [1], heat conduction [2], and water wave propagations [3]. In semiconductor device modeling, Helmholtz's equation arises frequently as an intermediate step in the solution of the nonlinear Poisson's problem. To solve these problems diverse numerical methods have been reported which include, finite difference [4], finite element [5], and boundary integral method (BIM) [6], [7], and [8]. Using these conventional methods, it has been found that fine grids and a large number of elements must be employed to get satisfactory accuracy [3]. This requires large computer core storage, and more computational time especially for the iteration scheme of the nonlinear Poisson's problem where the value at each grid point needs to be updated at each step of the iteration. Further, the BIM formulations are in most cases limited to homogeneous Helmholtz's equation and tied closely to the particular problem at hand [6]. In this paper, a simple approach to solve the homogeneous and nonhomogeneous Helmholtz's equation is proposed. The technique is based on the computation of Laplacian potential by the method of moments (MoM) [9], without resorting to different formulations using Hankel functions as it is commonly done in BIM [10]. Besides its generality to solve Laplace's, Poisson's, and Helmholtz's equations in one single code implementation, the present method will considerably reduce the number of domain grids compared to the finite difference methods and does not require any interpolation. The accuracy of the MoM solution will be compared to the solutions of finite difference method (FDM) and finite element method (FEM), using ELLPACK implementation [4].

II. Mathematical Formulation of MoM

Consider the following expression as the governing elliptic equation for a smooth function Ψ defined in a 2-D region $\Re$, with contour C

$$\nabla^2\Psi(x, y) + \lambda(x, y)\Psi(x, y) = F(x, y) \tag{1}$$

where λ and F are known functions on the domain $\Re$. The general form of (1) includes, as specializations, the following cases:

1) Laplace's equation, with $\lambda = 0$ and $F = 0$.
2) Poisson's equation, with $\lambda = 0$ and $F \neq 0$.
3) Helmholtz's equation, with $\lambda \neq 0$ and $F \neq 0$.

So only one general formulation addresses the solution to all of the three cases above. On the contour C the boundary condition can be of Dirichlet, Neuman, or mixed type, as given by the general form

$$\alpha\Psi + \beta\frac{\partial\Psi}{\partial n} = \gamma \tag{2}$$

where α, β, and γ, are known spatial functions. Further, $\partial\Psi/\partial n$ represents the normal derivative. It is implied that consistent boundary conditions are chosen.

The proposed scheme to solve the given boundary value problems starts by assuming the term $\lambda\Psi$ as a known function, and including it with the given function F, reducing (1) to the familiar Poisson's equation

$$\nabla^2\Psi(x, y) = -G(x, y) \tag{3}$$

with

$$G(x, y) = \lambda(x, y)\Psi(x, y) - F(x, y). \tag{4}$$

The solution to Poisson's equation in (3) can be expressed as

$$\Psi = \phi_h + \phi_p \tag{5}$$

where ϕ_h is the solution to the homogeneous Poisson's equation (Laplace's equation)

$$\nabla^2\phi_h = 0 \tag{6}$$

and ϕ_p is the particular integral, i.e.,

$$\nabla^2\phi_p = -G(x, y). \tag{7}$$

Here we use the particular solution of the Poisson's equation given by [12]

$$\phi_p(x, y) = \frac{1}{2\pi}\iint_{\Re} G(x', y') \cdot \ln\left(\frac{k}{\sqrt{(x - x')^2 + (y - y')^2}}\right) dx'\,dy' \tag{8}$$

Manuscript received January 6, 1995; revised August 1, 1995. This work was supported in part by the CASE Center of Syracuse University.

The authors are with the Electrical and Computer Engineering Department, Syracuse University, Syracuse, New York 13244-1240 USA.

IEEE Log Number 9414840.

where (x, y) and (x', y') denote the spatial coordinates of the field and source points, respectively, and k is an arbitrary constant. k is taken as 100 in the present work, since for 2-D problem the reference potential at infinity is not zero but finite. A value of $k = 100$, provides the potential value at infinity. To evaluate the above integral we divide the domain $\mathfrak{R}$ into N sub-regions. The midpoint coordinates of each of the sub-regions $\Delta\mathfrak{R}_i$ are denoted by (x_{2i}, y_{2i}). Then the potential ϕ_p at the field point (x, y) is approximated by

$$\phi_p(x, y) \cong \sum_{i=1}^{N} G(x_{2i}, y_{2i}) a_i(x, y) \tag{9}$$

where

$$a_i(x, y) = \frac{1}{2\pi} \iint_{\Delta\mathfrak{R}_i} \cdot \ln\left(\frac{k}{\sqrt{(x-x')^2 + (y-y')^2}}\right) dx'\, dy'. \tag{10}$$

Hence it is assumed that $G(x, y)$ is constant within each subregion $\Delta\mathfrak{R}_i$ and is equal to the value $G(x_{2i}, y_{2i})$.

An expression similar to (9) can be derived to approximate the Laplacian potential ϕ_h. The potential ϕ_h can be assumed to be produced by some equivalent charge sources, σ, located on the contour C [12]. Then the potential ϕ_h at any point (x, y) can be obtained from $\sigma(x, y)$ using the following integral [9]

$$\phi_h(x, y) = \frac{1}{2\pi} \int_C \sigma(x', y') \ln\left(\frac{k}{\sqrt{(x-x')^2 + (y-y')^2}}\right) dl' \tag{11}$$

where l' is the arc length on the contour C.

The boundary condition of the homogeneous potential ϕ_h is obtained from (2) and (5) as

$$\alpha\phi_h + \beta\frac{\partial\phi_h}{\partial n} = \gamma - \left(\alpha\phi_p + \beta\frac{\partial\phi_p}{\partial n}\right). \tag{12}$$

It can be seen that (6) along with the boundary condition of (12), constitute the same boundary-value problem as the one considered in [9]. Hence an approximate solution to (11) can be obtained by the MoM. Pulse-expansion and point-matching techniques will be adopted to solve the present problem. If the contour C is segmented by M straight lines of length ΔC_i between points i and $i + 1$, then σ can be represented by the step approximation

$$\sigma = \sum_{i=1}^{M} \sigma_i P_i(l) \tag{13}$$

where $P_i(l)$ is a pulse function equal to 1 on ΔC_i and zero elsewhere and σ_i is its unknown amplitude. Substituting (13) into (11), we obtain an approximation for ϕ_h

$$\phi_h(x, y) \cong \sum_{i=1}^{M} \sigma_i c_i(x, y) \tag{14}$$

where

$$c_i(x, y) = \int_{\Delta C_i} \ln\left(\frac{k}{\sqrt{(x-x')^2 + (y-y')^2}}\right) dl'. \tag{15}$$

Using (4), (9) and (14), the Helmholtz potential Ψ at an arbitrary point field (x, y) can now be expressed as

$$\Psi(x, y) = \sum_{i=1}^{M} \sigma_i c_i(x, y) + \sum_{i=1}^{N} (\lambda_i \Psi_i - F_i) a_i(x, y) \tag{16}$$

where for simplicity we used the abbreviations $\lambda_i = \lambda(x_{2i}, y_{2i}), F_i = F(x_{2i}, y_{2i})$, and $\Psi_i = \Psi(x_{2i}, y_{2i})$ in (4).

$\Psi(x, y)$ in (16) can be evaluated once the unknown terms, σ_i and Ψ_i, are determined. Next a system of two matrix equations is derived and solved for σ_i and Ψ_i. The first matrix equation of this system is readily obtained by satisfying (16) at the midpoints (x_{2j}, y_{2j}) of each of the N subregion $\Delta\mathfrak{R}_i$. Using matrix notation, we obtain

$$[\Psi_j] = [p_{ji}] \cdot [\sigma_i] + [q_{ji}] \cdot [\lambda_i \Psi_i - F_i] \tag{17}$$

where $p_{ji} = c_i(x_{2j}, y_{2j})$, and $q_{ji} = a_i(x_{2j}, y_{2j})$.

The second matrix equation is obtained by enforcing the boundary condition of (12) as follows. We define $\hat{r}_j = (x_j, y_j), j = 1, 2, \ldots, M$, as the midpoints of ΔC_j. The boundary conditions are enforced at each $\hat{r}_j$. Substitution of (9) and (14) into (12) gives the following set of equations

$$\sum_{i=1}^{M} \sigma_i l_{ji} = \gamma_j - \sum_{i=1}^{N} (\lambda_i \Psi_i - F_i) b_{ji} \qquad j = 1, 2, \ldots, M \tag{18}$$

where $\gamma_j = \gamma(\hat{r}_j)$ and

$$l_{ji} = \left(\alpha c_i + \beta\frac{\partial c_i}{\partial n}\right)_{(x, y) = \hat{r}_j} \tag{19}$$

$$b_{ji} = \left(\alpha a_i + \beta\frac{\partial a_i}{\partial n}\right)_{(x, y) = \hat{r}_j} \tag{20}$$

(18) is conveniently expressed in matrix notations as

$$[l_{ji}][\sigma_i] = [\gamma_j] - [b_{ji}][\lambda_i \Psi_i - F_i]. \tag{21}$$

Observe that (17) and (21) form a system of two equations in two unknowns which can be solved for σ_i and Ψ_i. We use (21) to obtain an expression for σ and then substitute it into (17), and after simple matrix manipulations the following equation for Ψ_i is obtained

$$[A] \cdot [\Psi_i] = [B] \tag{22}$$

where

$$[A] = [I] + ([p_{ji}][l_{ji}]^{-1}[b_{ji}] - [q_{ji}])[\lambda_i] \tag{23}$$

$$[B] = [p_{ji}][l_{ji}]^{-1}[\gamma_j] + ([p_{ji}][l_{ji}]^{-1}[b_{ji}] - [q_{ji}])[F_i] \tag{24}$$

and $[I]$ denotes the $N \times N$ identity matrix.

From the last three equations some general comments can be made:

1) Analytic expressions can be easily derived for the evaluation of all the terms in matrices $[A]$ and $[B]$ that

include the integrals (10) and (15). In the next section the evaluation of the relevant matrix elements will be presented.

2) The matrix $[l_{ji}]$ has the moment matrix elements similar to the matrix elements obtained in [9]. For different Helmholtz problems with the same boundary conditions, $[l_{ji}]$ remains unchanged. This observation is important in an iteration scheme where the boundary conditions are kept the same.
3) Problems with multiple right-hand sides are solvable with minimum additional computational time since the function F in (17) appears only as a term of matrix $[B]$ in (24).
4) The domain and the contour discretization schemes are totally independent. This feature can offer the flexibility to handle boundary discontinuities without the need of excessive domain grid generations. This will be illustrated through numerical examples in Section IV.
5) Once Ψ_i is determined at the grid points, using Gaussian elimination for instance, the potential at any other point, is obtained using ordinary matrix multiplications as shown by (17). No interpolations are needed.

III. Evaluation of the Matrix Elements

To compute the function Ψ from (17), one has to evaluate the integrals of the matrix elements in (19) and (20). The evaluation of the one-dimensional integral in (19) for the l_{ji} matrix elements has been discussed in [9]. Complex-function theory was found useful to evaluate the integrals of (19) the kernel of which is either a Green's function or its gradient. The Green's function has integrable logarithmic singularities. The integral of the gradient, $\partial c_i/\partial n$, is discontinuous at ΔC_i, equal to π internal to C, and equal to $-\pi$ external to C.

In this section the b_{ji} matrix elements will be evaluated. From (20) b_{ji} is determined once the integrals of a_i and $\partial a_i/\partial n$ are both computed. The $\partial a_i/\partial n$ integral has no logarithmic kernel and can be easily evaluated. The two-dimensional integral of a_i can be evaluated by using the results of [9], as illustrated below. For simplicity we consider the rectangular subregion $\Delta\mathfrak{R}_i$ with coordinate system shown in Fig. 1. We will use the notation $z(x, y) = x + jy$ to represent a point in space. Referring to Fig. 1, the integral of (10) can be written as

$$a_i = \frac{1}{2\pi}\int_{y_i}^{y_{i+1}} dy' \int_{x_i}^{x_{i+1}} \ln\left(\frac{k}{|r-r'|}\right) dx' \tag{25}$$

where

$$|r-r'| = \sqrt{(x-x')^2 + (y-y')^2} \tag{26}$$

r and r' denote the radius vectors to the field and the source points, respectively. Using the identities

$$\ln\left(\frac{k}{|r-r'|}\right) = \mathrm{Re}\left(\ln\left(\frac{k}{z-z'}\right)\right) \tag{27}$$

and

$$dl' = |dz'| = dz'/u \tag{28}$$

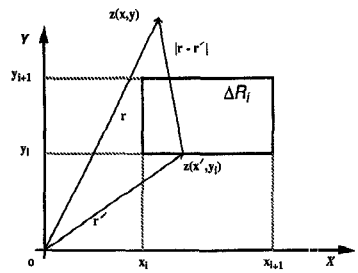

Fig. 1. Coordinate system for the evaluation of the matrix element integrals.

where u is the unit tangent to C. The integral in (25) can now be written as

$$a_i = \frac{1}{2\pi}\int_{y_i}^{y_{i+1}} I_{1i}\, dy' \tag{29}$$

where

$$I_{1i} = \mathrm{Re}\left(\frac{1}{u_{1i}}\int_{z(x_i,\, y_i)}^{z(x_{i+1},\, y_i)} \ln\left(\frac{k}{z-z'}\right) dz'\right) \tag{30}$$

I_{1i} has the same form as the matrix element integral evaluated in [9], and it is equal to

$$I_{1i} = \mathrm{Re}\left(\Delta i\left(1 + \ln\left(\frac{k}{z-z_{i+1}}\right)\right) + \frac{z_{i+1}-z_i}{u_{1i}}\left(\ln\left(\frac{z-z_{i+1}}{z-z_i}\right)\right)\right) \tag{31}$$

where $z_i = z(x_i, y_i), z_{i+1} = z(x_{i+1}, y_i), \Delta i = |z_{i+1} - z_i|$, and

$$u_{1i} = \frac{z_{i+1}-z_i}{\Delta i} = \frac{x_{i+1}-x_i}{|x_{i+1}-x_i|}. \tag{32}$$

By substituting (31) into (29) and integrating, we obtain the following expression for a_i

$$a_i = \frac{1}{2\pi}\left(\Delta i(y_{i+1} - y_i + I_{2i}) + \frac{1}{u_{1i}}(I_{3i} - I_{4i})\right) \tag{33}$$

where

$$I_{2i} = \int_{y_i}^{y_{i+1}} \mathrm{Re}\left(\ln\left(\frac{k}{z-z_{i+1}}\right)\right) dy' \tag{34}$$

which can be written as

$$I_{2i} = \mathrm{Re}\left(\frac{1}{u_{2i}}\int_{z(x_{i+1},\, y_i)}^{z(x_{i+1},\, y_{i+1})} \ln\left(\frac{k}{z-z'_{i+1}}\right) dz'\right) \tag{35}$$

where

$$u_{2i} = \frac{z(x_{i+1}, y_{i+1}) - z(x_{i+1}, y_i)}{|z(x_{i+1}, y_{i+1}) - z(x_{i+1}, y_i)|}. \tag{36}$$

Note that the integrals of (30) and (34) are similar except for the limits of integration. Hence (31) can also be used to compute I_{2i}.

The integral I_{3i}, which is defined as

$$I_{3i} = \int_{y_i}^{y_{i+1}} \mathrm{Re}\left((z-z_i)\ln\left(\frac{k}{z-z_{i+1}}\right)\right) dy' \tag{37}$$

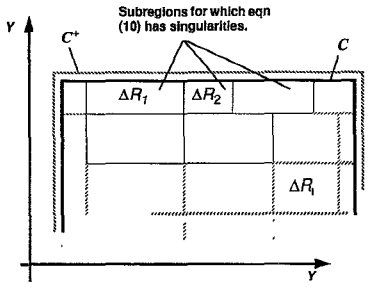

Fig. 2. Geometry modeling of the contour C^+.

can be expressed in terms of I_{2i} using complex-function theory as follows

$$I_{3i} = \int_{y_i}^{y_{i+1}} (x - x_i) \ln\left(\frac{k}{|z - z_{i+1}|}\right) dy' - \int_{y_i}^{y_{i+1}} (y - y') \operatorname{atan}\left(\frac{y - y'}{x - x_{i+1}}\right) dy'. \quad (38)$$

Using (34), the above integral becomes

$$I_{3i} = (x - x_i) I_{2i} + I_{0i} \quad (39)$$

where

$$I_{0i} = \int_{y-y_i}^{y-y_{i+1}} u \operatorname{atan}\left(\frac{u}{x - x_{i+1}}\right) du, \qquad u = y - y'. \quad (40)$$

I_{0i} can be evaluated analytically using integral tables. Finally, the integral I_{4i} in (33) is defined as

$$I_{4i} = \int_{y_i}^{y_{i+1}} \operatorname{Re}\left((z - z_i) \ln\left(\frac{k}{z - z_i}\right)\right) dy'. \quad (41)$$

Comparing (41) and (37), one can conclude that the integral I_{4i} can be obtained from the integral I_{3i} by simply replacing z_{i+1} by z_i in (37). Now all quantities of (25) are evaluated and can easily be programmed. However, as a word of caution, logarithmic singularities can appear when evaluating (25) for a subregion $\Delta\Re_i$ if one of its edges coincide with a ΔC_i segment of the contour C, as shown in Fig. 2. Probably the easiest technique to circumvent this type of singularity predicaments is to first move the ΔC_i segment locations to a fictious parallel surface C^+ just outside the bounding surface C [12].

IV. Numerical Applications

Example 1) Water Propagation: General numerical tests have been performed to show the validity of the present method. As a first example, we consider the problem of water propagation in a rectangular basin 100m×100m [3]. Denoting by Ψ the water evaluation, then the wave propagation is governed by (1) with $F = 0$, and $\lambda = k^2$ where k is the wave number. The boundary conditions used are displayed in Fig. 3. The solution by MoM is compared to the solutions obtained by FDM and FEM for various mesh sizes inside the domain. The minimum number of nodes required for each method to converge to the exact solution at any arbitrary point is optimized. Fig. 4 compares the solutions computed along

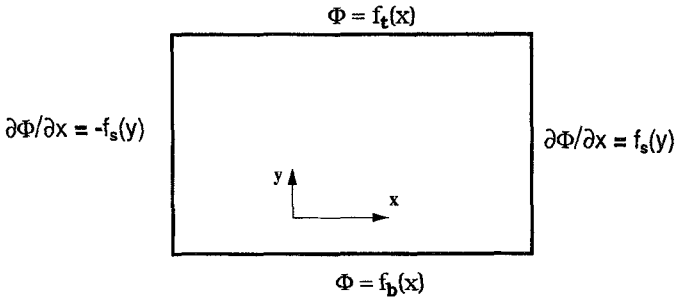

where $f_t(x) = \begin{cases} \cos(\alpha x) & \text{if } 20 \le x \le 80 \\ -2 & \text{if } x < 20 \\ 1 & \text{if } x > 80 \end{cases}$

$f_s(x) = \sin(\alpha y)$, $f_b = \cos(\alpha x)$, and $\alpha = 2\pi$

Fig. 3. Structure and boundary conditions of example 1.

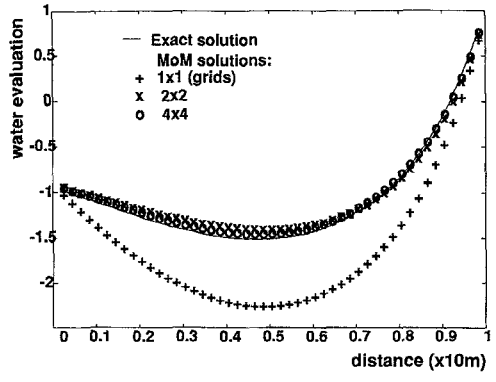

Fig. 4. MoM solutions for example 1.

the line $x = 90$ by the method of moments utilizing (1×1), (2×2) and (4×4) grids. Fig. 5 shows the solutions obtained by the finite element method utilizing (5×5), (10×10), and (20×20) grids. Fig. 6 shows the results obtained by the finite difference method utilizing (5×5), (15×15), and (35×35) grids. In all these figures, the solid line represents the exact solution. Referring to these figures, one can easily observe that a considerably smaller number of nodes are employed with the present method than with the conventional methods. The minimum number of the domain nodes required to obtain a satisfactory accuracy using MoM is 16 (4×4), compared to 400 (20×20) for FEM or up to 1000 nodes for FDM.

Example 2—MOST Modeling: The nonlinear Poisson's equation plays a key role in numerical modeling of semiconductor devices. Many important characteristics of VLSI devices can be extracted from the solution of Poisson's equation. The most common approach to the numerical solution of the nonlinear Poisson's equation is based on the application of Newton's method to simultaneous discretized equations [15]. This approach often requires large storage, especially for fine meshes as it is the case for two-dimensional modeling of the MOST [14].

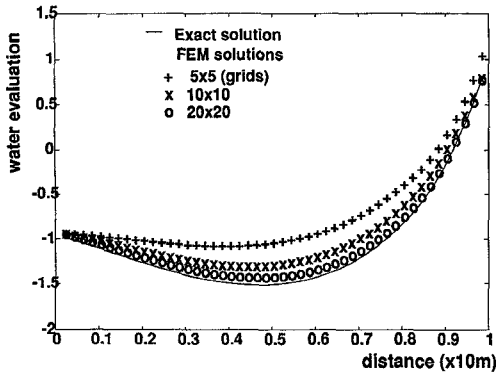

Fig. 5. FEM solutions for example 1.

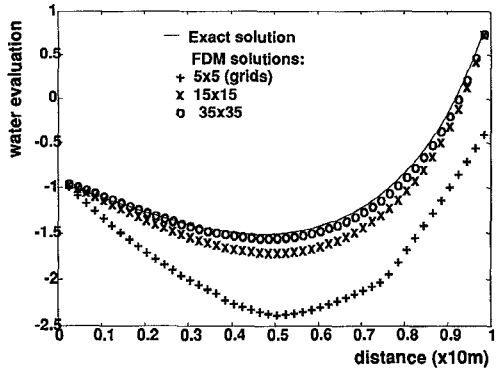

Fig. 6. FDM solutions for example 1.

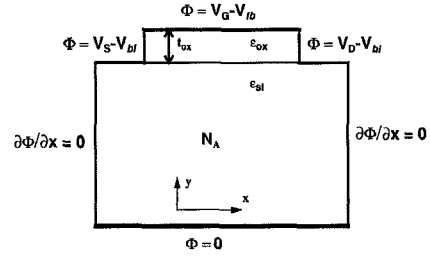

Fig. 7. Structure and boundary conditions of example 2.

In this section the MoM is applied to solve the nonlinear Poisson's equation that arises in the MOST modeling. We consider the MOST structure of Fig. 7 made on a p-type substrate with doping N_A. Under the low current approximation the potential Φ is governed by the Poisson's equation [16]

$$\frac{\partial^2\Psi}{\partial x^2}+\frac{\partial^2\Psi}{\partial y^2}=-\frac{n_i}{L_D^2}\left(e^{-\Psi}-e^{\Psi}-\frac{N_A}{n_i}\right) \tag{42}$$

where $\Psi = \Phi/V_T$ is the normalized potential. V_T is the thermal potential, n_i is the intrinsic carrier concentration, and L_D is the Debye length.

The boundary conditions adopted along the edges of the device are the same as those used by [16], [12], and are displayed in Fig. 7. On the oxide-semiconductor interface the following boundary condition is assumed

$$\epsilon_{ox}\frac{V_G-\Phi-V_{FB}}{t_{ox}}=\epsilon_s\frac{\partial\Phi}{\partial y} \tag{43}$$

where ϵ_{ox}, and ϵ_s are, respectively, the oxide and silicon permittivities. V_{FB} is the flat band voltage, and t_{ox} is the oxide thickness.

To solve the above elliptic problem we proceed first by dividing the boundary into M segments. Finer segments are used on the top edge of the device to handle its boundary discontinuities. Using the boundary conditions, and the technique described in [9], matrix $[l_{ji}]$ is computed, then inverted and stored. Independently, the base domain is also divided into N finite elements or cells. We seek to determine the electric potential at each midpoint of the cells using (42) which is nonlinear. To solve it we set up an iterative procedure, based on Newton's linearization [15]. At the K^{th} iteration we replace the right-hand side of (42) by its Fourier expansion about Ψ^k. Then the following Helmholtz's equation is obtained

$$\frac{\partial^2\Psi^{(k+1)}}{\partial x^2}+\frac{\partial^2\Psi^{(k+1)}}{\partial y^2}-G(\Psi^{(k)})\Psi^{(k+1)}=F(\Psi^{(k)}) \tag{44}$$

where F and G are given by

$$F(\Psi^{(k)})=\frac{n_i}{L_D^2}\left((\Psi^{(k)}+1)e^{-\Psi^{(k)}}+(\Psi^{(k)}-1)e^{\Psi^{(k)}}-\frac{N_A}{n_i}\right) \tag{45}$$

$$G(\Psi^{(k)})=\frac{n_i}{L_D^2}(e^{-\Psi^{(k)}}+e^{\Psi^{(k)}}). \tag{46}$$

The iteration scheme starts by taking some initial guess value for $\Psi^{(0)}$ so that (44) can be solved for the first approximation $\Psi^{(1)}$. Then $\Psi^{(1)}$ is used to find the second approximation $\Psi^{(2)}$. The procedure is repeated until the norm $\|\Psi^{(k+1)}-\Psi^{(k)}\|$ is less than a desired tolerance. However, this iteration scheme often diverges [13], [15], and some damping factor was found necessary to improve the convergence of the iterative solution. At the beginning of the K^{th} iteration step, the following formula was used for all inner nodes

$$\Psi^{(k+1)}=(1-R)\Psi^{(k-1)}+R\Psi^{(k)} \tag{47}$$

where $R(<1)$ is the relaxation factor.

The accuracy of the solution obtained by the present technique is demonstrated by comparison to the FDM (5-point) solution. For both methods, MoM and FDM, we let the values of the electric potential to be updated at each mesh point by means of explicit formula, that is, without the solution of simultaneous algebraic equations [15]. We assign $\Psi = 0$, as an initial guess, for all inner nodes. Once the convergence is attained for the domain nodes, then the electric potential at any other point in the device is determined by matrix multiplication as shown in (17), and without the need of any interpolation. For numerical computations, the relevant data used are as follows: the oxide thickness, $t_{ox} = 0.5$ μm. The flat band voltage, $V_{FB} = -1$ V, the doping profile is assumed uniform, $N_A = 10^{18}$ cm^{-3}, $n_i = 1.5 \times 10^{10}$ cm^{-3}, thermal potential, $V_T = 0.0258$ V, and $R = 0.1$. The results of the computations are shown in Fig. 8, where the distribution of the electric potential at the thermal equilibrium is plotted along different lines parallel to the x axis. The solid lines represent the solution obtained using the FDM and (o) symbol is reserved for the solutions obtained by the present method.

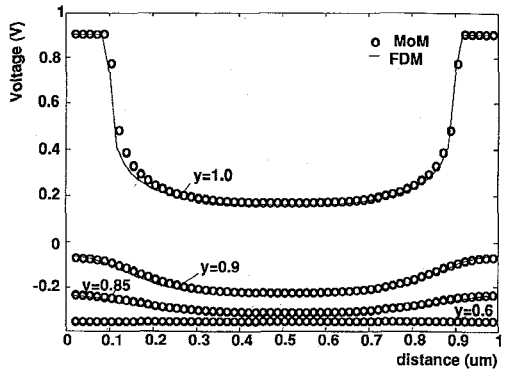

Fig. 8. The distribution of electric potentials along the lines parallel to the x-axis.

Close agreements can be observed between the two methods. However, for FDM 721 nonuniform mesh points are employed to reduce the total number of nodes (for uniform meshes over 4900 (70×70) nodes ought to be used). Finer meshes were chosen in the depletion region and near the junctions to resolve the fast variation of the electric potential [16] and the surface discontinuities. Whereas for MoM the number of the uniform meshes was 529 (23×23) or 400 for nonuniform cells. The number of iterations required for the convergence was 51 with the present technique compared to 108 iterations with FDM to reach the point at which the absolute maximum between two subsequent iterations was less than 0.05 (tolerance).

V. Conclusion

An efficient technique based on MoM formulation for solving a general Helmholtz equation has been presented. The main feature of this new formulation is the boundary conditions are satisfied independent of the region node discretizations. This feature was found specially useful when the boundary conditions have discontinuities. Considerable reduction in the domain grids are realized with the present method compared to the conventional methods such as finite difference method or the finite element methods.

References

[1] L. G. Copley, "Fundamental results concerning integral representation in acoustic radiation," *J. Acoust. Soc. Am.*, vol. 44, pp. 28–32, 1968.
[2] R. A. Altenkirch, M. Rezayat, R. Eichhorn, and F. J. Rizzo, "A study of heat conduction forward of flame in solids, by the boundary integral equation method," *Trans. ASME Ser. C. J. Heat Transfer,* vol. 104, pp. 734–740, 1982.
[3] M. Kawahara and K. Kashiyama, "Boundary type finite element method for surface wave motion based on the trigonometric function interpolation," *Int. J. Numer. Meth. Eng.*, vol. 21, pp. 1833–1852, 1985.
[4] J. R. Rice and R. F. Boisvert, *Solving Elliptic Problems Using ELLPACK.* New York: Springer-Verlag, 1985.
[5] P. L. Arlett, A. K. Bahrani, and O. C. Zienkiewicz, "Application of finite elements to the solution of Helmholtz's equation," *Proc. IEE,* vol. 115, no. 12, pp. 1762–1766, 1968.
[6] M. Rezayat, F. J. Rizzo, and D. J. Shippy, "A unified boundary integral equation method for class of second order elliptic boundary value problems," *J. Austral. Math. Soc. Ser.*, vol. B-25, pp. 501–517, 1984.
[7] K. Nagaya, and T. Yamaguchi, "Method for solving eigenvalue problems of the Helmholtz equation with an arbitrary shaped outer boundary and a number of eccentric inner boundaries of arbitrary shape," *J. Acoust. Soc. Am.*, vol. 90, pp. 2146–2153, 1991.
[8] P. J. Harris, "A boundary element method for Helmholtz equation using finite part integration," *Comp. Meth. Appl. Mech. Eng.*, vol. 95, pp. 331–342, 1992.
[9] R. F. Harrington, K. Pontoppidan, P. Abrahamsen, and N. C. Abertsen, "Computation of Laplacian potentials by an equivalent source method," *Proc. IEE,* vol. 116, no. 10, pp. 1715–1720, 1969.
[10] C. A. Brebbia, *The Boundary Element Method for Engineers.* New York: Wiley, 1978.
[11] R. F. Harrington, *Field Computation by Moment Methods.* New York: Macmillan, 1968.
[12] E. Arvas, R. I. Turkman, and P. S. Neelakantaswamy, "MOSFET analysis through numerical solution of Poisson's equation by the method of moments," *Solid-State Elect.*, vol. 30, no. 12, pp. 1355–1361, 1987.
[13] G. De Mey, "The boundary element method for modelling semiconductor components under low current approximation," in *Proc. Int. Conf. Simulation of Semiconductor Devices and Processes,* Pineridge Press, 1984, pp. 261–266.
[14] W. Fichtner, D. J. Rose, and R. E. Bank, "Semiconductor device simulation," *IEEE Tran. Electron. Devices,* vol. ED-30, no. 9, pp. 1018–1030, 1983.
[15] W. F. Ames, *Nonlinear Partial Differential Equations in Engineering.* New York: Academic, 1965.
[16] J. D. Kendall and A. R. Boothroyd, "A two-dimensional analytical threshold voltage model for MOSFET's with arbitrarily doped substrates," *IEEE Electron Device Lett.*, vol. EDL-7, pp. 401–403, 1986.

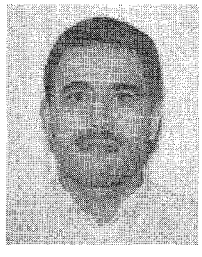

Jalel Rejeb was born on August 10, 1962 in Moknine, Tunisia. He received the B.S. and M.S. degrees in electrical engineering from Syracuse University, Syracuse, NY, in 1985 and 1987, respectively.

From 1988 to 1990 he worked in the Kassimi Arch, Bouzid, Tunisia. He is currently a Ph.D. candidate in the Department of Electrical and Computer Engineering at Syracuse University. His primary area of research is in the simulation of semiconductor devices and numerical methods in electromagnetic problems.

Mr. Rejeb has been a recipient of the National Tunisian Scholarship from 1981 to 1987.

Tapan Sarkar (S'69–M'76–SM'81–F'92), photograph and biography not available at the time of publication.

Ercument Arvas (M'85–SM'89) received the B.S. and M.S. degrees from Middle East Technical University, Ankara, in 1976 and 1979, and the Ph.D. degree from Syracuse University in 1983, all in electrical engineering.

From 1977 to 1979 he was employed by TESTAS Electronics Co., Ankara, where he worked as a Project Engineer in the Communication Group. Between 1979 and 1982 he was a Research Assistant in the Electrical and Computer Engineering Department of Syracuse University, where his research interest involved PO, GTD, and the application of the method of moments to low frequency scattering problems. He was a Visiting Assistant Professor at the same department during spring 1983. During the period of 1983 to 1984 he was an Assistant Professor in the Electrical Engineering Department of Yildiz University in Istanbul. From 1984 to 1987 he was with the Electrical Engineering Department of Rochester Institute of Technology. He joined the Electrical and Computer Engineering Department of Syracuse University in the fall of 1987 and presently he is a Professor in the same department. His current research interest is in the development of numerical and analytical techniques in electromagnetic theory and signal processing.

Dr. Arvas is a member of Eta Kappa Nu.